Sparse Matrix/Canonical Grid Method Applied to 3-D Dense Medium Simulations

Benjamin E. Barrowes, Chi O. Ao, Fernando L. Teixeira, and Jin A. Kong

Abstract— **The Sparse Matrix/Canonical Grid (SMCG) method, which has been shown to be an efficient method for calculating the scattering from 1-D and 2-D random rough surfaces, is extended to 3-D dense media scattering. In particular, we study the scattering properties of media containing randomly positioned and oriented dielectric spheroids. Mutual interactions between scatterers are formulated using a Method of Moments (MoM) solution of the volume integral equation. Iterative solvers for the resulting system matrix normally require $\mathcal{O}(N^2)$ operations for each matrix-vector multiply. The SMCG method reduces this complexity to $\mathcal{O}(N \log N)$ by defining a neighborhood distance, r_d, by which particle interactions are decomposed into "strong" and "weak". Strong interaction terms are calculated directly requiring $\mathcal{O}(N)$ operations for each iteration. Weak interaction terms are approximated by a multivariate Taylor series expansion of the 3-D background dyadic Green's function between any given pair of particles. Greater accuracy may be achieved by increasing r_d, using a higher order Taylor expansion, and/or increasing mesh density at the cost of more interaction terms, more FFTs, and longer FFTs, respectively. Scattering results, computation times, and accuracy for large-scale problems with r_d up to 2 gridpoints, 14×14×14 canonical grid size, fifth order Taylor expansion, and 15000 discrete scatterers are presented and compared against full solutions.**

Keywords— **3-D scattering, SMCG, fast methods, random media, spheroid**

I. Introduction

ELECTROMAGNETIC scattering from and wave propagation in three-dimensional (3-D) discrete random media has been a topic of continued research due to its broad range of applications. For instance, in applications related to the remote sensing of the environment, the characterization of the electromagnetic wave interaction with natural media is of great importance. Natural media (e.g., snow, ice, and soil) often consist of a large number of densely packed, electrically small discrete scatterers that are randomly distributed in some background host medium (discrete random media). Moreover, many artificial materials (e.g., particulate composites) can also be characterized as being composed of randomly distributed scatterers in a host medium. Even some materials which can in principle be conceptualized and realized by regular, periodic arrangements, are often subject to random perturbations, both in terms of the positions, sizes and/or constitutive properties of the discrete scatterers.

For dense random media, several analytical methods based on wave theory, such as the quasi-crystalline approximation (QCA [1, 2]), the quasi-crystalline approximation with coherent potential (QCA-CP [3]), or other approximations such as independent scattering and Foldy's approximation [4], are frequently employed. These analytical methods rely on basic simplifying assumptions about the media, such as tenuous media (low permittivity and permeability contrast), sparse media (low fractional volume of scatterers, typically less than 5%), or particle shape (*e.g.* spherical). These assumptions facilitate tractable analytical solutions but are not able to capture the essential physics of many real world problems. Moreover, it is often difficult to assess the range of validity of such analytical techniques *a priori*.

The alternative approach to deal with more complex media problems in a systematic manner is to resort to numerical techniques. Numerical methods such as the Method of Moments (MoM [5]), the finite difference time domain (FDTD [6, 7]), and related ones have allowed a partial relaxation of some of the limiting assumptions concerning the medium [8, 9]. In particular, the MoM provides a self-consistent solution which includes multiple interactions between discrete particles through an interaction (impedance) matrix $\overline{\overline{Z}}$. The main disadvantages of the MoM are the computation time required for solving the often large and dense resulting system of equations and the computer memory requirements for the storage of $\overline{\overline{Z}}$.

To help alleviate these bottlenecks, several so-called fast numerical methods have been developed in recent years for both 2-D and 3-D electromagnetic problems (e.g. [3, 10–16]). One of these fast methods, the Sparse Matrix/Canonical Grid (SMCG) method [13,14,17–20], speeds up the solution of certain electromagnetic problems by decomposing the interaction matrix $\overline{\overline{Z}}$ into two separate matrices: a strong interaction matrix $\overline{\overline{Z}}^{\mathrm{s}}$ which contains the interactions of nearby elements calculated exactly, and a weak interaction matrix $\overline{\overline{Z}}^{\mathrm{w}}$ which contains an approximation of the weaker interaction terms from elements located farther apart. In contrast to Fast Multipole Methods (FMM), this procedure does not group interactions together, but rather approximates each individual weak interaction based on a canonical grid. The strong interaction matrix tends to be sparse while the vast majority of

Benjamin E. Barrowes and Jin A. Kong are with the Research Laboratory of Electronics and Department of Electrical Engineering and Computer Science, Massachusetts Institute of Technology, Cambridge, MA 02139-4307

Chi O. Ao is with the Department of Physics and Research Laboratory of Electronics, Massachusetts Institute of Technology, Cambridge, MA 02139-4307

Fernando L. Teixeira is with the ElectroScience Laboratory and Department of Electrical Engineering, The Ohio State University, Columbus, OH 43210-1272

This work was supported by the Office of Naval Research (ONR) under contract numbers N00014-99-1-0175, N00014-01-1-0713, DTRS-57-98-D-00043, and DACA-89-99-K-0006, and through a NSF Graduate Fellowship.

the interactions between elements are included in the weak interaction matrix. This latter matrix can be derived by a Taylor series expansion around a canonical grid [14, 20] or through the use of translation addition theorems [3, 17]. The advantage in doing this is that during the solution of $\overline{\overline{Z}}$ using iterative solvers (as is frequently the case), the original full matrix-vector multiply $\overline{\overline{Z}} \cdot \overline{x}$ ($\mathcal{O}(N^2)$ complexity) may be replaced by a sparse matrix multiply, $\overline{\overline{Z}}^{\mathrm{s}} \cdot \overline{x}$ ($\mathcal{O}(N)$) plus a Fast Fourier Transform (FFT) assisted multiply $\overline{\overline{Z}}^{\mathrm{w}} \cdot \overline{x}$ ($\mathcal{O}(N \log N)$). This FFT assisted matrix-vector multiply is possible because of the multilevel block Toeplitz (MBT) structure inherent in $\overline{\overline{Z}}^{\mathrm{w}}$ as a result of the canonical grid expansion of the weak interactions.

In this paper, we extend the SMCG method to 3-D case and consider its application to the scattering from complex media consisting of a collection of randomly positioned and oriented dielectric spheroids in a homogeneous host medium. In Section II, we describe the MoM formulation of $\overline{\overline{Z}}$ derived from a many-body volume integral equation. In Section III, we describe the 3-D SMCG method in detail, including a discussion on the various tradeoffs associated with choosing the method parameters as well as the Taylor series expansion of the background dyadic Green's function around the canonical grid gridpoints. In Section IV, scattering results from these collections of spheroids calculated by the SMCG method are presented and compared to results obtained from the full MoM solution. Computation times, memory requirements, and accuracy for the approximated and full MoM solutions for cases of 500–15000 particles, varying neighborhood distances, Taylor series expansion orders of 0-5, and grids of 6×6×6 to 14×14×14 are also considered in Section IV. This is followed by conclusions in Section V.

II. Formulation

The electric field $\overline{E}(\overline{r})$ in a random medium consisting of N arbitrary dielectric objects (discrete scatterers) with permittivity $\epsilon(\overline{r}'_j)$ excited by an incident electric field $\overline{E}_{inc}(\overline{r})$ can be described by the volume integral equation (VIE) [21] through a summation over each scatterer, i.e.,

$$\overline{E}(\overline{r}) = \overline{E}_{inc}(\overline{r}) + \frac{k^2}{\epsilon} \sum_{j=1}^{N} \int_{V'_j} dV'_j \; (\epsilon(\overline{r}'_j) - \epsilon) \, \overline{\overline{G}}(\overline{r}, \overline{r}'_j) \cdot \overline{E}(\overline{r}'_j), \tag{1}$$

where V_j is the volume of scatterer j, k is the wavenumber of the homogeneous background medium, ϵ is the permittivity of the background medium, $\epsilon(\overline{r}'_j)$ is the permittivity inside the j^{th} scatterer. $\overline{\overline{G}}(\overline{r}, \overline{r}'_j)$ is the background generalized dyadic Green's function whose principal value is given by

$$\overline{\overline{G}}(\overline{r}, \overline{r}'_j) = \left[\overline{\overline{I}} + \frac{\nabla\nabla}{k^2} \right] g(\overline{r}, \overline{r}'_j), \tag{2}$$

which, to account for the singularity encountered when $\overline{r} = \overline{r}'_j$, should be written as [3, 22, 23]

$$\overline{\overline{G}}(\overline{r}, \overline{r}'_j) = P.V. \overline{\overline{G}}(\overline{r}, \overline{r}'_j) - \frac{\overline{\overline{L}} \delta(\overline{r} - \overline{r}'_j)}{k^2}. \tag{3}$$

where $P.V.$ stands for Principal Value. The exclusion volume dependent term in Eq. (3) becomes important when calculating the self interaction terms (see below). Finally, $g(\overline{r}, \overline{r}'_j)$ is the scalar Green's function,

$$g(\overline{r}, \overline{r}'_j) = \frac{e^{ik|\overline{r} - \overline{r}'_j|}}{4\pi |\overline{r} - \overline{r}'_j|}. \tag{4}$$

Primed variables indicate those variables pertaining to the scatterers while unprimed variables indicate quantities positioned outside the scatterers (background or host medium). The induced polarization inside each object due to the electric field at $\overline{r}'_j$ is given by $\overline{P}(\overline{r}'_j) = (\epsilon(\overline{r}'_j) - \epsilon)\overline{E}(\overline{r}'_j)$ (from Eq. (1)).

To solve Eq. (1) using the Method of Moments (MoM), the electric field inside the each particle is expanded in a set of N_b basis functions, *e.g.* for the j^{th} particle,

$$\overline{E}(\overline{r}'_j) = \sum_{\alpha=1}^{N_b} c_{j\alpha} \, \overline{f}_{j\alpha}(\overline{r}'_j). \tag{5}$$

The basis functions $\overline{f}_{j\alpha}(\overline{r}_j)$ for each particle can be chosen based on particle size and geometry as detailed later on. For our purposes, we will also assume that these basis functions are orthonormal:

$$\int_{V'_j} dV'_j \; \overline{f}_{j\alpha}(\overline{r}'_j) \cdot \overline{f}_{j\beta}(\overline{r}'_j) = \delta_{\alpha\beta}, \tag{6}$$

where $\delta_{\alpha\beta}$ is the Kronecker delta.

To find the field inside each object, we substitute Eq. (5) into Eq. (1) to arrive at

$$\left[\sum_{\beta=1}^{N_b} c_{i\beta} \, \overline{f}_{i\beta}(\overline{r}'_i) \right] = \overline{E}_{inc}(\overline{r}'_i) \quad + \\ \frac{k^2}{\epsilon} \sum_{j=1}^{N} \int_{V'_j} dV'_j \; (\epsilon(\overline{r}'_j) - \epsilon) \, \overline{\overline{G}}(\overline{r}'_i, \overline{r}'_j) \cdot \left[\sum_{\alpha=1}^{N_b} c_{j\alpha} \, \overline{f}_{j\alpha}(\overline{r}'_j) \right]. \tag{7}$$

By invoking the orthonormality of the basis functions [Eq. (6)] and applying Galerkin's technique, Eq. (7) can be written as:

$$c_{i\beta} = \int_{V'_i} dV'_i \; \overline{f}_{i\beta}(\overline{r}'_i) \cdot \overline{E}_{inc}(\overline{r}'_i) + \sum_{j=1}^{N} \sum_{\alpha=1}^{N_b} c_{j\alpha} z_{ij,\alpha\beta}, \tag{8}$$

where

$$z_{ij,\alpha\beta} = B_{j\alpha} \int_{V'_i} dV'_i \int_{V'_j} dV'_j \; \overline{f}_{i\beta}(\overline{r}'_i) \cdot \overline{\overline{G}}(\overline{r}'_i, \overline{r}'_j) \cdot \overline{f}_{j\alpha}(\overline{r}'_j), \tag{9}$$

with

$$B_{j\alpha} = \frac{k^2}{\epsilon} (\epsilon(\overline{r}'_j) - \epsilon). \tag{10}$$

The first term on the right hand side of Eq. (7) is determined by the incident field and is known for a given configuration while the other two terms describe the interaction matrix $\overline{\overline{Z}}$ with $c_{j\alpha}$ forming the unknown excitation

vector $\overline{x}$. Suppose that the self term (that is, $i=j$, $\alpha=\beta$ term) in Eq. (8) is (see [8])

$$z_{ij,\alpha\beta}|_{i=j,\alpha=\beta} = C_{i\beta}, \tag{11}$$

then Eq. (8) can be recast into the matrix equation

$$\overline{\overline{Z}} \cdot \overline{x} = \overline{b}, \tag{12}$$

where

$$\overline{b} = \begin{bmatrix} \begin{bmatrix} \int_{V_1'} dV_1' \, \overline{f}_{11}(\overline{r}_1') \cdot \overline{E}_{inc}(\overline{r}_1') \\ \int_{V_1'} dV_1' \, \overline{f}_{12}(\overline{r}_1') \cdot \overline{E}_{inc}(\overline{r}_1') \\ \vdots \\ \int_{V_1'} dV_1' \, \overline{f}_{1N_b}(\overline{r}_1') \cdot \overline{E}_{inc}(\overline{r}_1') \end{bmatrix} \\ \vdots \\ \begin{bmatrix} \int_{V_N'} dV_N' \, \overline{f}_{N1}(\overline{r}_N') \cdot \overline{E}_{inc}(\overline{r}_N') \\ \int_{V_N'} dV_N' \, \overline{f}_{N2}(\overline{r}_N') \cdot \overline{E}_{inc}(\overline{r}_N') \\ \vdots \\ \int_{V_N'} dV_N' \, \overline{f}_{NN_b}(\overline{r}_N') \cdot \overline{E}_{inc}(\overline{r}_N') \end{bmatrix} \end{bmatrix}. \tag{13}$$

Similarly

$$\overline{x} = \Big[[c_{11}, c_{12}, \ldots, c_{1N_b}], \ldots, [c_{N1}, c_{N2}, \ldots, c_{NN_b}] \Big]^T, \tag{14}$$

and the $N_b \times N_b$ block of $\overline{\overline{Z}}$ which describes the interaction between particles i and j is given by

$$\overline{\overline{Z}}_{ij} = \begin{cases} -\begin{bmatrix} z_{ij,11} & z_{ij,12} & \cdots & z_{ij,1N_b} \\ z_{ij,21} & z_{ij,22} & & \\ \vdots & & \ddots & \vdots \\ z_{ij,N_b1} & & \cdots & z_{ij,N_bN_b} \end{bmatrix} & i \neq j, \\ \begin{bmatrix} (1-C_{i1}) & 0 & \cdots & 0 \\ 0 & (1-C_{i2}) & & \\ \vdots & & \ddots & \vdots \\ 0 & & \cdots & (1-C_{iN_b}) \end{bmatrix} & i = j, \end{cases} \tag{15}$$

where $\overline{\overline{Z}}$ is then understood to be

$$\overline{\overline{Z}} = \begin{bmatrix} \overline{\overline{Z}}_{11} & \overline{\overline{Z}}_{12} & \cdots \\ \vdots & \ddots & \vdots \\ \overline{\overline{Z}}_{N_b1} & \cdots & \overline{\overline{Z}}_{N_bN_b} \end{bmatrix}. \tag{16}$$

The size of $\overline{\overline{Z}}$ is $N_bN \times N_bN$, and the lengths of vectors $\overline{x}$ and $\overline{b}$ are N_bN. The calculation of the self terms $C_{i\beta}$ are based on the electrostatic solution of spheroids and are described in detail in [8] Appendix A.

In this paper, we consider identical prolate spheroidal particles at arbitrary locations and with arbitrary orientations. Assuming electrically small particles, we choose the basis functions to be the electrostatic solutions to the Laplace equation for a prolate spheroid. The interaction equation, Eq. (12), was derived above to show the generality of the method: for particles of different shapes, one need only choose appropriate basis functions (as many as needed) in order to calculate scattering from the collection. Also note that each individual particle need not be identical for the method described in Section III to be valid. Each particle may differ in shape, size, permittivity, *etc.* as long as the particle remains small enough compared to the wavelength (size parameter $ka \ll 1$) so that its response to $\overline{E}_{inc}(\overline{r})$ may be accurately modeled by a point response. For reference, the first three basis functions for the spheroid corresponding to the dipole solutions of the Laplace equation are given as

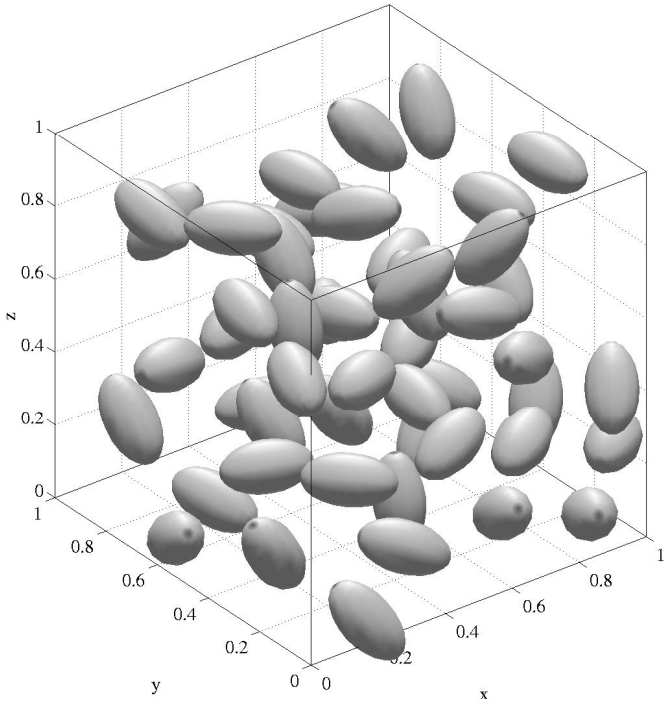

Fig. 1. Densely packed medium consisting of 50 dielectric spheroids. Elongation=1.8, f_v=0.1.

$$\overline{f}_{j1} = \hat{z}_{bj} \frac{1}{\sqrt{v_j}}, \tag{17a}$$

$$\overline{f}_{j2} = \hat{x}_{bj} \frac{1}{\sqrt{v_j}}, \tag{17b}$$

$$\overline{f}_{j3} = \hat{y}_{bj} \frac{1}{\sqrt{v_j}}. \tag{17c}$$

Here, $\hat{x}_{bj}$, $\hat{y}_{bj}$, and $\hat{z}_{bj}$ are the principal axes of spheroid j. For the expressions of the higher order basis functions and further details concerning this MoM solution for the case of small prolate spheroids, the reader is referred to [8]. An example of one realization of a random medium filled with 30 spheroids with elongation $e = 1.8$, and fractional volume $f_v = 0.3$, contained a unit cube test volume is illustrated in Fig. 1.

III. 3-D SMCG Method

Consider a medium filled with many discrete scatterers (*e.g.* spheroids, as in Fig. 1) at random positions and with

random orientations contained in a cubic test volume. The dielectric spheroids have a statistical distribution realized by a shuffling process described in [8]. After a suitable distribution of N_{cube} particles is generated, the collection may be truncated to any shape. In our case we will truncate to a spherical test volume consisting of N_{sphere} particles.

A. SMCG Model Parameters

The Sparse Matrix/Canonical Grid (SMCG) method achieves reduced complexity and reduced memory requirements by assuming that scatterers are small enough so that accuracy is maintained though only point interactions are considered, and by decomposing the interaction matrix $\overline{\overline{Z}}$ into two separate matrices: the "strong" and "weak" interaction matrices. This decomposition is governed by a neighborhood distance, r_d, beyond which radius interactions are considered weak. The choice of the neighborhood distance is discussed in more detail in Section III-B.

If the particles are small compared to the wavelength of the incident radiation, the induced electric field inside the particle can be considered constant and may therefore be accurately modeled by a dipole response located at the center of the particle. In this case, the integrals in Eqs. (7)-(13) may be replaced by the volume of that particle as:

$$\int_{V_i'} dV_i' \rightsquigarrow v_i = \frac{4}{3}\pi a_i^2 c_i, \tag{18}$$

where a_j is the length of the semiminor axis and $c_j = a_j e_j$ with e_j being the elongation or aspect ratio. The assumptions stated above allow the separation of $\overline{\overline{Z}}$ into three distinct matrices: 1) a pre-multiplying basis function matrix $\overline{\overline{f}}_i$ dependent on particle i, 2) the Green's function kernel $\overline{\overline{G}}(\overline{r}_i', \overline{r}_j')$ (which now only depends on the distance separating the centers of particles i and j, R_{ij} [see Eq. (23)]), and 3) a post-multiplying basis function matrix $\overline{\overline{f}}_j$ dependent on j. In rectangular coordinates this becomes

$$\overline{\overline{Z}}_{ij} = \overline{\overline{f}}_i \cdot \overline{\overline{G}}(\overline{r}_i', \overline{r}_j') \cdot \overline{\overline{f}}_j \tag{19}$$

where

$$\overline{\overline{f}}_i = \begin{bmatrix} f_{i1,x} & f_{i1,y} & f_{i1,z} \\ \vdots & \vdots & \vdots \\ f_{iN_b,x} & f_{iN_b,y} & f_{iN_b,z} \end{bmatrix} \tag{20}$$

and

$$\overline{\overline{G}}(R_{ij}) = \begin{bmatrix} G_{xx}(R_{ij}) & G_{xy}(R_{ij}) & G_{xz}(R_{ij}) \\ G_{yx}(R_{ij}) & G_{yy}(R_{ij}) & G_{yz}(R_{ij}) \\ G_{zx}(R_{ij}) & G_{zy}(R_{ij}) & G_{zz}(R_{ij}) \end{bmatrix}. \tag{21}$$

Note that $\overline{\overline{f}}_j$ is the transpose of $\overline{\overline{f}}_i$ if i=j. If ξ denotes x, y, or z, then the terms of Eq. (21) are

$$G_{\xi_1\xi_2}(R_{ij}) = g(R_{ij})\delta_{\xi_1\xi_2} + \frac{1}{k^2}\frac{\partial^2}{\partial\xi_1\partial\xi_2} g(R_{ij}), \tag{22}$$

where $g(R_{ij})$ is the scalar Green's function [Eq. (4)], again $\delta_{\xi_1\xi_2}$ is the Kronecker delta, and

$$R_{ij} = \sqrt{(x_i - x_j)^2 + (y_i - y_j)^2 + (z_i - z_j)^2}. \tag{23}$$

If $\overline{\overline{f}}$ is constructed by inserting $\overline{\overline{f}}_i$ into the appropriate columns (determined by gridpoint index) and rows (determined by particle index), then Eq. (19) can be expanded to include all particle interactions as

$$\overline{\overline{Z}} = \overline{\overline{f}} \cdot \overline{\overline{G}} \cdot \overline{\overline{f}}^{\mathrm{T}}, \tag{24}$$

where $\overline{\overline{f}}^{\mathrm{T}}$ denotes the transpose of $\overline{\overline{f}}$. Note that $\overline{\overline{f}}$ is sparse, while $\overline{\overline{G}}$ is a dense, $(NN_b) \times (NN_b)$ matrix containing the exact interactions between every pair of particles.

The next step in the SMCG method involves approximating the weak interaction between particles i and j in the interaction matrix $\overline{\overline{Z}}$ by a multivariate Taylor series expansion of $\overline{\overline{G}}(R_{ij})$ about the gridpoints nearest to the particles i and j, respectively. Let this approximated matrix be $\overline{\overline{Z}}^{\mathrm{w}}$ defined according to the following. Let a cubic lattice be superimposed onto the test volume with $N_{g,x}$, $N_{g,y}$, and $N_{g,z}$ lattice points, or gridpoints, in the x, y, and z dimensions respectively. For all of the simulations considered in this paper,

$$N_{g,x} = N_{g,y} = N_{g,z} = N_g \tag{25}$$

with

$$N_{g,i} = \frac{(i-1) + \frac{1}{2}}{N_g} \tag{26}$$

for gridpoints located in a unit cube. The spacing between gridpoints is then $\Delta r_g = 1/N_g$. All those interactions located further apart than the predetermined neighborhood distance are considered "weak" interactions. Thus, decomposing $\overline{\overline{Z}}$ through the relation

$$\overline{\overline{G}} = \overline{\overline{G}}(\mathcal{R}_s) + \overline{\overline{G}}^{\mathrm{cg}}(\mathcal{R}_w), \tag{27}$$

for all $i, j = 1 \ldots N$ where $\mathcal{R}_s$ denotes the set of distances between pairs of particles whose interactions are considered strong, and $\mathcal{R}_w$ is a set containing all other pair interactions (considered weak), Eq. (19) can be written as

$$\begin{aligned} \overline{\overline{Z}} &= \overline{\overline{Z}}^{\mathrm{s}} + \overline{\overline{Z}}^{\mathrm{w}} \\ &= \underbrace{\overline{\overline{f}} \cdot \overline{\overline{G}}(\mathcal{R}_s) \cdot \overline{\overline{f}}^{\mathrm{T}}}_{\overline{\overline{Z}}^{\mathrm{s}}} + \underbrace{\overline{\overline{f}} \cdot \overline{\overline{G}}^{\mathrm{cg}}(\mathcal{R}_w) \cdot \overline{\overline{f}}^{\mathrm{T}}}_{\overline{\overline{Z}}^{\mathrm{w}}} \end{aligned} \tag{28}$$

where the superscript "cg" denotes an approximation based on the distance between the particle and its associated gridpoint located at $\overline{r}_g$. $\mathcal{R}_s$ and $\mathcal{R}_w$ are mutually exclusive sets with $\mathcal{R}_s \bigcup \mathcal{R}_w = R$. $\overline{\overline{G}}(\mathcal{R}_s)$ contains the exact Green's function between particles only in close proximity (closer than r_d) while all other entries are set to 0. $\overline{\overline{G}}(\mathcal{R}_s)$ is the same size as $\overline{\overline{G}}$ from Eq. (24), but is sparse. $\overline{\overline{G}}^{\mathrm{cg}}(\mathcal{R}_w)$ is also the same size as $\overline{\overline{G}}$ and contains an approximation of the remaining weak interactions. $\overline{\overline{G}}^{\mathrm{cg}}(\mathcal{R}_w)$ is actually a sum of as many matrices as is required for the expansion (see Table II). The derivation of $\overline{\overline{G}}^{\mathrm{cg}}(\mathcal{R}_w)$ as well as fast methods for the subsequent matrix-vector multiply will be discussed below.

B. Parameter Considerations

A natural question at this point is: beyond what distance should interactions be considered "weak"? The distance at which the separation occurs is called the neighborhood distance (r_d) and is defined in terms of the number of gridpoints away from the gridpoint of interest. It is clear that the choice for r_d influences both the accuracy of the results using the SMCG method and the computation time required. On one hand, for small r_d (< 1 inter-gridpoint space Δr_g), approximation errors tend to accumulate and cause the iterative solver of Eq. (28) either to not converge or converge to incorrect values. On the other hand, a large r_d causes a greater number of interactions to be classified as "strong" and the SMCG method reverts to a full iterative approach. Reasonable r_d values from simulations are between 1 and 2 gridpoints.

The neighborhood distance must be defined in terms of gridpoints because for weak interactions, particles interact through the Green's function matrix $\overline{\overline{G}}^{\mathrm{cg}}(\mathcal{R}_w)$ which is defined only in terms of the number of gridpoints and their respective locations (see Section III-C). Thus, all particles associated with gridpoints closer than r_d (measured with respect to the inter-gridpoint distance) will have strong interactions with the particle under consideration, while those particles associated with gridpoints which are located further away than r_d are classified as weak interactions. In this way, r_d defines the strong interaction cloud (or molecule) which is illustrated in Fig. 2 for three spheroids S_1, S_2, and S_3 with $N_g = 3$. Table I lists the number of gridpoints included in the strong interaction cloud (g_{r_d}) for the first few ranges of r_d.

Range of r_d (# of Δr_g)	g_{r_d}
$0<r_d\leq 1$	1
$1<r_d\leq\sqrt{2}$	7
$\sqrt{2}<r_d\leq 2$	19
$2<r_d\leq\sqrt{5}$	33
$\vdots$	

TABLE I

NUMBER OF SURROUNDING GRIDPOINTS, g_{r_d}, INCLUDED IN THE STRONG INTERACTION CLOUD AS A FUNCTION OF NEIGHBORHOOD DISTANCE r_d.

One related question is, how fine or coarse of a grid is necessary or optimum for a given collection of scatterers? At the very least, there must be as many or fewer undulations (local extrema) in $\overline{\overline{G}}$ between gridpoints as the order of the Taylor series expansion (γ) for it to be possible for $\overline{\overline{G}}^{\mathrm{cg}}$ to approximate $\overline{\overline{G}}$ adequately. In terms of computation time, the number of multiplies M^s required during each iteration of the iterative solver for $\overline{\overline{Z}}^{\mathrm{s}} \cdot \overline{x}$ from Eq. (28) is $\mathcal{O}(N)$. M^s can be approximated as the average number of interactions with each particle from other particles associated with the same gridpoint, multiplied by the number of gridpoints in the strong interaction cloud, and multiplied again by the number of spheroids, *i.e.*

$$M^s = N\left(\frac{N}{N_g^3}\right) g_{r_d}. \tag{29}$$

Because $1/N_g^3 \ll 1$, M^s is $\mathcal{O}(N)$ unless N_g is small and/or g_{r_d} is large.

The number of multiplies M^w required during each iteration of the iterative solver for $\overline{\overline{Z}}^{\mathrm{w}} \cdot \overline{x}$ in Eq. (28) depends on the FFT length ($\approx 8N_g^3$ for $\overline{\overline{G}}^{\mathrm{cg}}(N_g)$, see Eq. (43)) and the number of expansion matrices (N_T, see Section III-C Table II). Thus, if we estimate the number of multiplies required for an N-length FFT as $N\log_2 N$, M^w is

$$M^w = 8N_g^3\left(\log_2(8N_g^3)\right) N_T. \tag{30}$$

Therefore, the total number of multiplies M for one iteration can be estimated by $M = M^w + M^s$. The N_g which minimizes this function can be found by solving the following transcendental equation for N_g given g_{r_d} and N_T,

$$\frac{-3N^2 g_{r_d}}{N_g^4} + 24N_g^2 N_T\left(\log_2(8N_g^3) + \frac{1}{\ln 2}\right) = 0. \tag{31}$$

Equation (31) provides an estimate of the number of gridpoints which minimizes computation time as a function of the neighborhood distance and the expansion order.

The approximation error due to the SMCG method decreases if a larger r_d is chosen because more terms are being

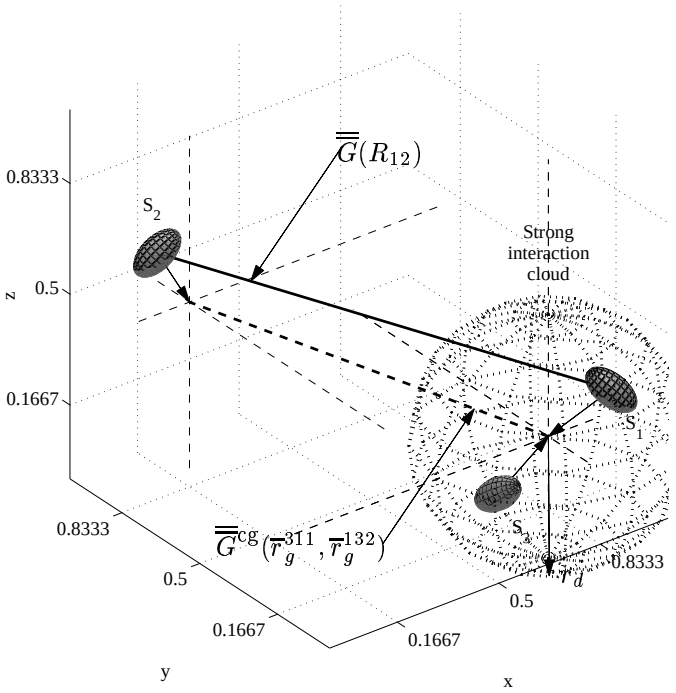

Fig. 2. Strong interaction cloud with r_d=1.1. Spheroids S_1 and S_3 are closest to the same gridpoint and thus their interaction is included in $\overline{\overline{Z}}^{\mathrm{s}}$. Spheroid S_2 is beyond r_d and thus its exact interactions with both S_1 ($\overline{\overline{G}}(R_{12})$ shown as a thick solid line between S_1 and S_2) and S_3 are approximated as $\overline{\overline{G}}^{\mathrm{cg}}(\overline{r}_g^{311}, \overline{r}_g^{132})$ and included in $\overline{\overline{Z}}^{\mathrm{w}}$.

counted in the strong interaction cloud and computed exactly. This error will also decrease if N_g is chosen larger because a finer mesh implies that the Taylor series will estimate functions over smaller regions. In other words, the Taylor approximation will have less error because it is fitted to a smoother function. The effect on computation time and accuracy of the expansion order, r_d, and N_g can be seen in the results listed in Table III.

C. 3-D Dyadic Green's Function Approximation

After the parameters of the 3-D SMCG method have been chosen, weak particle interactions are approximated by expanding the background dyadic Green's function about distance between the gridpoints nearest to each pair of particles. Let each particle located at $\overline{r}_i$ be associated with its nearest gridpoint $g^{l_i m_i n_i}$ located at $\overline{r}_g^{l_i m_i n_i}$ where l_i, m_i, and n_i are gridpoint indices in the x, y, and z dimensions respectively and are integers in the range

$$1 \le \{l_i, m_i, n_i\} \le N_g, \quad \forall \ i = 1, \ldots, N. \tag{32}$$

If particles i and j are associated with gridpoints $g^{l_i m_i n_i}$ and $g^{l_j m_j n_j}$ located at $\overline{r}_g^{l_i m_i n_i}$ and $\overline{r}_g^{l_j m_j n_j}$ respectively, $\overline{\overline{G}}(R_{ij})$, defined in rectangular coordinates by Eq. (21), can be approximated by a γ^{th} order Taylor series expansion $\overline{\overline{G}}^{\rm cg}$ as

$$\overline{\overline{G}}_{ij}^{\rm cg}(\mathcal{R}_w) = \sum_{\gamma=0}^{\infty} \left(\sum_{\xi=x,y,z} \Delta\xi_{ij} \frac{\partial}{\partial \xi} \right)^{\gamma} \frac{\overline{\overline{G}}(\overline{r}_g^{l_i m_i n_i}, \overline{r}_g^{l_j m_j n_j})}{\gamma!}, \tag{33}$$

or via the trinomial theorem as

$$\overline{\overline{G}}_{ij}^{\rm cg}(\mathcal{R}_w) = \sum_{\gamma=0}^{\infty} \sum_{\gamma_x+\gamma_y+\gamma_z=\gamma} \left(\frac{1}{\gamma_x!\gamma_y!\gamma_z!} \right) \times \left\{ \prod_{\xi=x,y,z} (\Delta\xi_{ij})^{\gamma_\xi} \right\} \frac{\partial^{\gamma_x}}{\partial x^{\gamma_x}} \frac{\partial^{\gamma_y}}{\partial y^{\gamma_y}} \frac{\partial^{\gamma_z}}{\partial z^{\gamma_z}} \overline{\overline{G}}(\overline{r}_g^{l_i m_i n_i}, \overline{r}_g^{l_j m_j n_j}) \tag{34}$$

where

$$\begin{aligned} \Delta\xi_{ij} &= \Delta\xi_i - \Delta\xi_j \\ &= (\overline{r}_{i,\xi} - \overline{r}_{g,\xi}^{l_i m_i n_i}) - (\overline{r}_{j,\xi} - \overline{r}_{g,\xi}^{l_j m_j n_j}), \end{aligned} \tag{35}$$

and again ξ is a placeholder for x, y, or z. $\overline{\overline{G}}^{\rm cg}(\mathcal{R}_w)$ from Eq. (28) is realized by Eq. (33) over all values of i and j and depends only on gridpoint locations $\overline{r}_g$ and the *relative* distance of each particle from its associated gridpoint.

Note that the relative distances $\Delta\xi_i$ in Eq. (33), are the only quantities which are particle specific and that they are scalars. Accordingly, we move these particle dependent quantities into $\overline{\overline{f}}$ by multiplying $\overline{\overline{f}}_i$ by $\Delta\xi_i$ over $\overline{\overline{f}}$ (*c.f.* Eqs. (19)-(24)), *i.e.*

$$\overline{\overline{f}}_{\gamma_x\gamma_y\gamma_z} \equiv \left(\prod_{\xi=x,y,z} (\Delta\xi_i)^{\gamma_\xi} \right) \overline{\overline{f}}_i, \quad \forall \ i = 1..N. \tag{36}$$

The remaining terms in Eq. (34) are dependent only upon the gridpoints, we define

$$\overline{\overline{G}}_{\gamma_x\gamma_y\gamma_z} \equiv \left(\frac{1}{\gamma_x!\gamma_y!\gamma_z!} \right) \frac{\partial^{\gamma_x}}{\partial x^{\gamma_x}} \frac{\partial^{\gamma_y}}{\partial y^{\gamma_y}} \frac{\partial^{\gamma_z}}{\partial z^{\gamma_z}} \overline{\overline{G}}(\overline{r}^{\Delta l \Delta m \Delta n}) \tag{37}$$

where $\overline{\overline{G}}(\overline{r}^{\Delta l \Delta m \Delta n})$ is an $3N \times 3N$ matrix defined by Eq. (21) with R_{ij} defined by Eq. (23) being the distance between gridpoints located at $\overline{r}_g^{l_i m_i n_i}$ and $\overline{r}_g^{l_j m_j n_j}$. Because of the translational invariance of the dyadic Green's function, the entries of $\overline{\overline{G}}(\overline{r}^{\Delta l \Delta m \Delta n})$ depend only on the differential number of gridpoints Δl, Δm, and Δn if the ordering of l, m, and n are sequential along the axes.

The i subscript in Eq. (36) corresponds to a pre-multiplication of $\overline{\overline{G}}_{\gamma_x\gamma_y\gamma_z}$ and can be thought of as a "source" particle from which radiation is being emitted, while the similar post-multiplication matrix corresponding to the j subscript would be $\overline{\overline{f}}^{\rm T}_{\gamma_x\gamma_y\gamma_z}$ and is analogous to a "sink" particle with an induced electric field caused (in part) by particle i.

Using the definitions above, we can now expand the weak interaction matrix $\overline{\overline{Z}}^{\rm w}$ as

$$\begin{aligned} \overline{\overline{Z}}^{\rm w} &= \overline{\overline{f}} \cdot \overline{\overline{G}}^{\rm cg}(\mathcal{R}_w) \cdot \overline{\overline{f}}^{\rm T} \\ &= \sum_{\gamma=0}^{\infty} \sum_{\gamma_x+\gamma_y+\gamma_z=\gamma} \overline{\overline{Z}}^{\rm w}_{\gamma_x\gamma_y\gamma_z} \end{aligned} \tag{38}$$

where

$$\overline{\overline{Z}}^{\rm w}_{\gamma_x\gamma_y\gamma_z} = \sum \sum \sum_{\begin{bmatrix} \gamma_{x_1}+\gamma_{x_2}=\gamma_x \\ \gamma_{y_1}+\gamma_{y_2}=\gamma_y \\ \gamma_{z_1}+\gamma_{z_2}=\gamma_z \end{bmatrix}} \Lambda \ \overline{\overline{f}}_{\gamma_{x_1}\gamma_{y_1}\gamma_{z_1}} \overline{\overline{G}}_{\gamma_x\gamma_y\gamma_z} \overline{\overline{f}}^{\rm T}_{\gamma_{x_2}\gamma_{y_2}\gamma_{z_2}} \tag{39}$$

and where

$$\Lambda = (-1)^{\gamma_{x_2}+\gamma_{y_2}+\gamma_{z_2}} \binom{\gamma_x}{\gamma_{x_2}} \binom{\gamma_y}{\gamma_{y_2}} \binom{\gamma_z}{\gamma_{z_2}}. \tag{40}$$

The γ_{ξ_1} and γ_{ξ_2} in Eq. (39) are integers which take on all combinations in the interval $[0, \gamma_\xi]$ which satisfy $\gamma_{\xi_1} + \gamma_{\xi_2} = \gamma_\xi$. For example, in the second order (γ=2) Taylor series expansion, $\overline{\overline{Z}}^{\rm w}$ would be approximated by 6 terms as

$$\overline{\overline{Z}}^{\rm w} \approx \overline{\overline{Z}}^{\rm w}_{200} + \overline{\overline{Z}}^{\rm w}_{110} + \overline{\overline{Z}}^{\rm w}_{101} + \overline{\overline{Z}}^{\rm w}_{020} + \overline{\overline{Z}}^{\rm w}_{011} + \overline{\overline{Z}}^{\rm w}_{002}, \tag{41}$$

and, for example, the γ_x=2, γ_y=0, γ_z=0 ($\overline{\overline{Z}}^{\rm w}_{200}$) term would be (from Eq. (39))

$$\overline{\overline{Z}}^{\rm w}_{200} = \overline{\overline{f}}_{200} \overline{\overline{G}}_{200} \overline{\overline{f}}^{\rm T}_{000} - 2\overline{\overline{f}}_{100} \overline{\overline{G}}_{200} \overline{\overline{f}}^{\rm T}_{100} + \overline{\overline{f}}_{000} \overline{\overline{G}}_{200} \overline{\overline{f}}^{\rm T}_{200} \tag{42}$$

with $\overline{\overline{f}}_{000} = \overline{\overline{f}}$ from Eq. (36). Lastly, if $(\epsilon(\overline{r}'_j) - \epsilon)$ is particle dependent, $\frac{k^2}{\epsilon}(\epsilon(\overline{r}'_j) - \epsilon)$ from Eq. (10) should also be multiplied into either the pre- or post- $\overline{\overline{f}}$ multiplication in a fashion similar to that of Eq. (36).

The reduction in computational complexity and memory requirements is realized by exploiting the structure inherent to $\overline{\overline{G}}_{\gamma_x\gamma_y\gamma_z}$. As mentioned earlier, the Green's function

matrix is highly redundant if the grid is ordered sequentially. In fact, $\overline{\overline{G}}_{\gamma_x\gamma_y\gamma_z}$ can be classified as a multilevel block Toeplitz (MBT) matrix with $M = 3$ levels, of size $N_{g,x}$, $N_{g,x}$, $N_{g,x}$ respectively, with the final level being a dense 3×3 block [24]. Matrix-vector multiplies of MBT matrices can be achieved in $\mathcal{O}(N_{FFT} \log N_{FFT})$ operations, instead of $\mathcal{O}(N^2)$, where N_{FFT} is the FFT length defined as

$$N_{FFT} = 9 \left(\prod_{\xi=x,y,z} (2N_{g,\xi} - 1) \right). \tag{43}$$

For each unique vector, the matrix-vector multiply involving an MBT matrix requires another FFT with length given by Eq. (43). In terms of Eq. (39), because $\overline{\overline{G}}_{\gamma_x\gamma_y\gamma_z}$ remains unchanged for the same N_g and background wavenumber k, the FFT of the expansion matrices $\overline{\overline{G}}_{\gamma_x\gamma_y\gamma_z}$ may be performed once and stored. Then for each step in the iterative solution, one FFT must be performed for each unique combination of $\overline{\overline{f}}^{\mathrm{T}}_{\gamma_{x_2}\gamma_{y_2}\gamma_{z_2}}$ and $\overline{x}$, and likewise an inverse FFT must be calculated for each unique $\overline{\overline{f}}_{\gamma_{x_1}\gamma_{y_1}\gamma_{z_1}}$. Table II lists the total number of transforms performed for a single $\overline{\overline{Z}}^{\mathrm{w}} \cdot \overline{x}$ multiply using the canonical grid expansion (N_T).

Expansion order (γ)	Number of expansion terms ($\overline{\overline{G}}_{\gamma_x\gamma_y\gamma_z}$)	N_T
0	1	2
1	3	8
2	6	20
3	10	40
4	15	70
5	21	112

TABLE II

NUMBER OF EXPANSION TERMS AND TOTAL NUMBER OF FFTS (BOTH FORWARD AND INVERSE) FOR EXPANSION ORDER γ.

Utilizing this 3-D SMCG method, the total complexity of solving Eq. (12) is reduced from $\mathcal{O}(KN^2)$ to $\mathcal{O}(KN_TN \log N)$ where K is the number of steps required for the iterative solver to converge. In Section IV, the 3-D SMCG method is shown to indeed realize results which require much less computation time while maintaining a desired tolerance.

IV. RESULTS

In this section, we apply the 3-D SMCG method to finding the scattering from a large collection of randomly distributed and oriented spheroids contained in a spherical test volume. Each of the N_{cube}=500–15000 spheroids considered are identical with respect to size, shape, and permittivity ($\epsilon(\overline{r}'_j)$). The size parameter ka for each spheroid is 0.2. Likewise, the fractional volume of the spheroids in the test volume is 20%. Only the dipole basis functions of Eq. (17) are employed, i.e., $N_b = 3$. Thus, there are a maximum of 45000 unknown coefficients $c_{j\alpha}$ to solve for. For a given N_{cube}, the same randomly generated configuration was used for all combinations of γ, r_d, and N_g. All results were computed on a Compaq Alphaserver DS20E with 4GB of RAM.

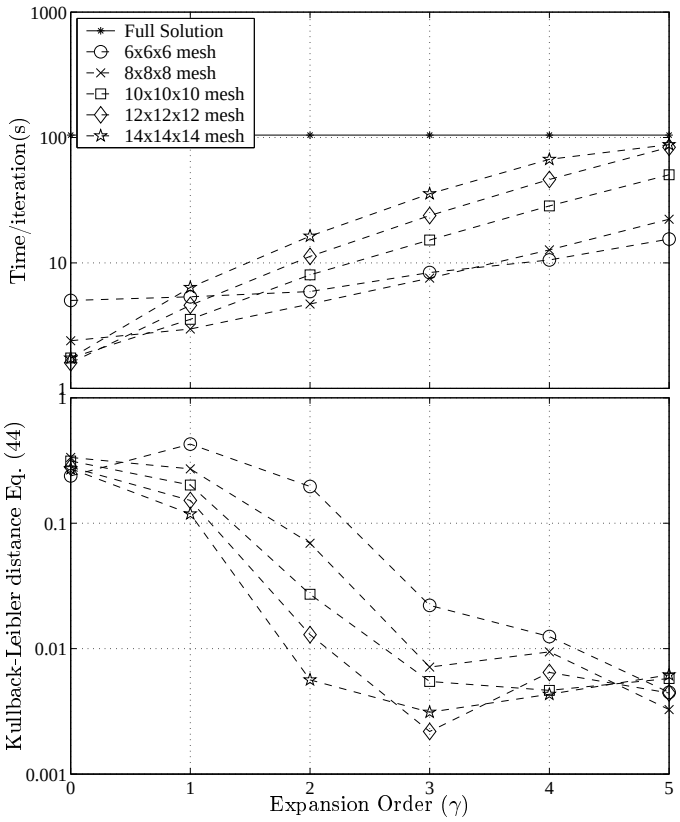

Fig. 3. Computation times and Kullback-Leibler distances for SMCG method for γ=0-5 with r_d=1.1Δr_g and N_{cube}=10000.

Four parameters dictate the resulting accuracy and computation time of the SMCG method as compared to the full MoM method. While the computation time of the full method depends only on the number of spheroids in the test volume N_{sphere}, the SMCG method additionally depends on the neighborhood distance r_d, the Taylor series expansion order γ, and the number of gridpoints N_g in each dimension. The relationship between expansion order and computation time and accuracy is illustrated in Fig. 3 where expansion orders from γ=0 to γ=5 were considered. Note that γ=0 corresponds physically to approximating all of the spheroids as actually being located at their respective (nearest) gridpoints.

As a measure of the "distance" of the approximated scattering results from those given by the full method, the Kullback-Leibler distance [25] is used, *i.e.*,

$$p(\sigma_T||\sigma) = \sum_{n=1}^{N_\theta} \left| \sigma_T(n) \log \frac{\sigma_T(n)}{\sigma(n)} \right| / N_\theta \tag{44}$$

where σ is the radar cross section (RCS) resulting from the full solution and σ_T is the approximated RCS calculated using the SMCG method. The RCSs are computed from

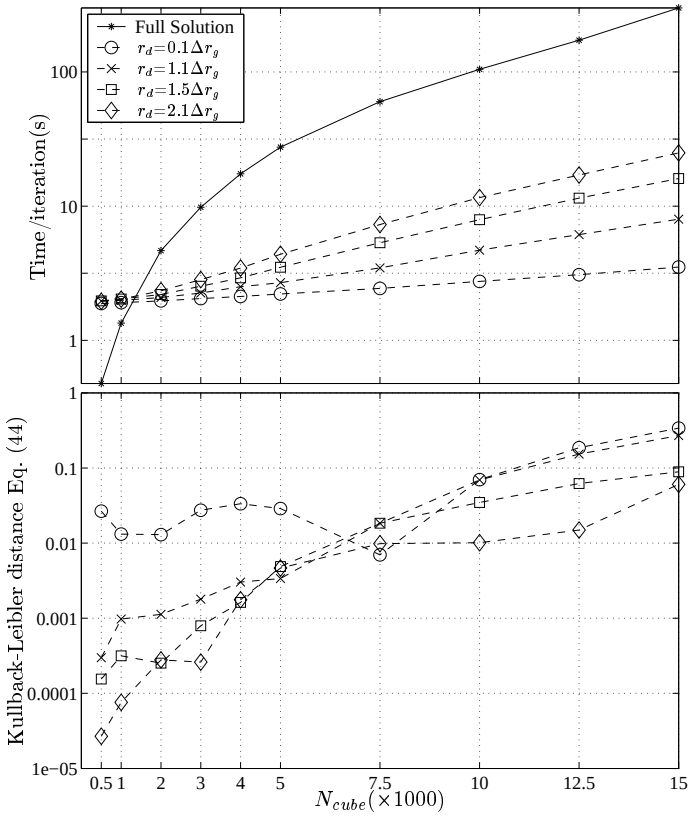

Fig. 4. Computation times and Kullback-Leibler distances for SMCG method for r_d=0.1–2.1Δr_g with γ=2 and N_g=8.

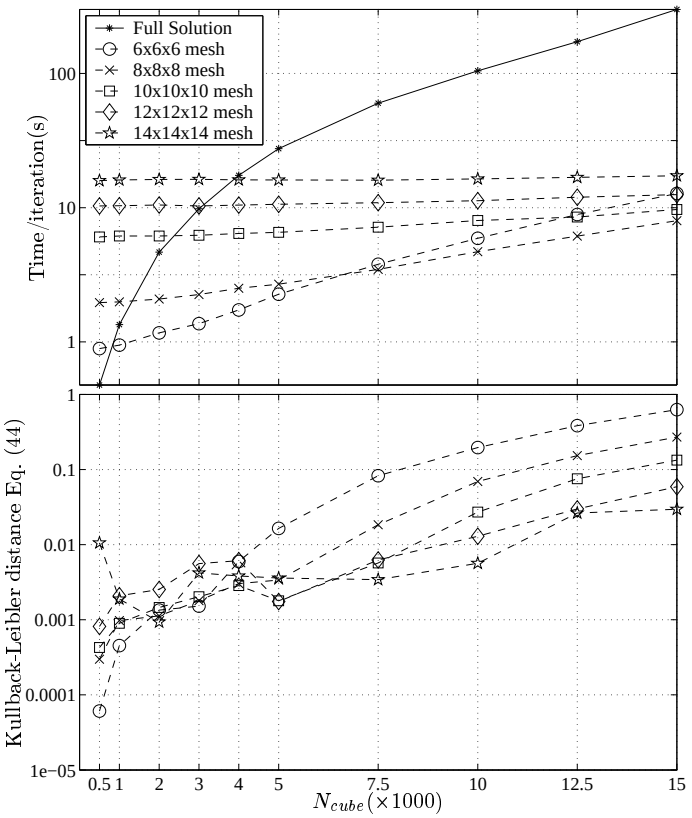

Fig. 5. Computation times and Kullback-Leibler distances for SMCG method for N_g=6–14 with γ=2 and r_d=1.1Δr_g.

the dipole excitation strengths [8] at N_θ=200 distinct angles. An example can be seen in Fig. 6. As expected, for increasing expansion order and grid size, computation time increases dramatically until it approaches the computation time of the full solution. However, for γ=2, most grid sizes maintain a small Kullback-Leibler distance, while realizing an substantial reduction in computation time.

The effect of varying the neighborhood distance r_d is shown in Fig. 4. As the neighborhood distance increases from 0.1Δr_g to 2.1Δr_g, the marginal speed of the SMCG method approaches the marginal speed of the full method (*i.e.* the slope of the curves are similar) due to many strong interactions being included in $\overline{\overline{Z}}^{\mathrm{s}}$ instead of being approximated in $\overline{\overline{Z}}^{\mathrm{w}}$. As a general trend, the Kullback-Leibler distance in Fig. 4 is smaller for larger r_d for the same reason.

Figure 5 shows computation times and Kullback-Leibler distances for the same set of data as Fig. 4 except that r_d is kept at r_d=1.1Δr_g, while the number of gridpoints is varied from $N_g = 6$ to $N_g = 14$. Note that for finer meshes, the FFT computation time dominates the overall computation time, which results in very flat curves with respect to N_{cube}. This also illustrates the tradeoff between grid size and the neighborhood distance discussed in more detail in Section III-B. The final figure, Fig. 6, shows the convergence of σ_T to σ for successively accurate model parameters, and Table III records pertinent computation times and Kullback-Leibler distances for a number of cases.

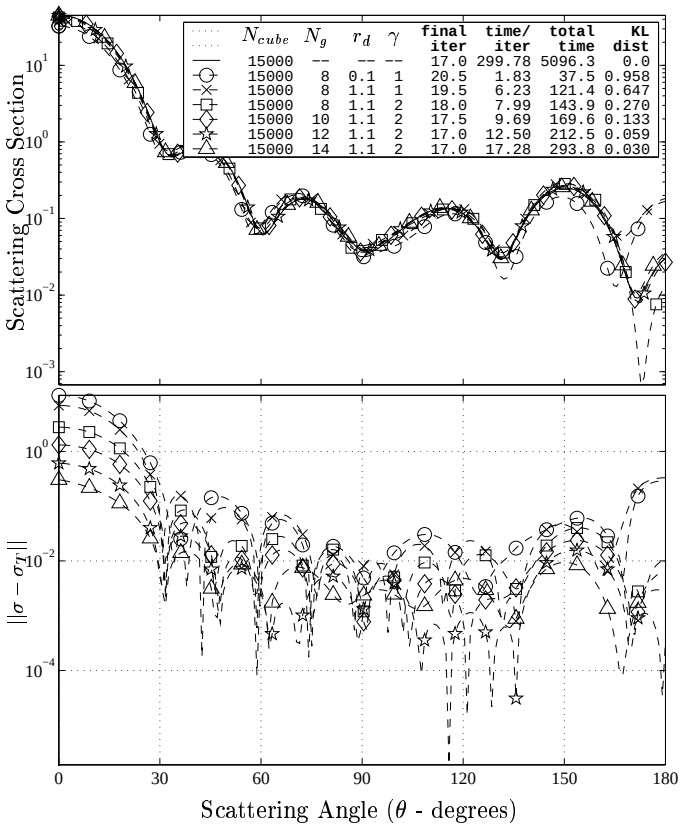

Fig. 6. Radar Cross Section (σ) for increasing accurate approximations.

	N_g	N_{FFT}	total iters	time/ iter	Eq. (44)	speed up
Neighborhood distance $r_d = 0.1\Delta r_g$ γ=1	6	11979	28.0	2.4	2.485	124.45
	8	30375	20.5	1.8	0.958	163.88
	10	61731	19.5	2.9	0.708	103.04
	12	109503	18.0	4.3	0.507	70.40
	14	177147	17.5	6.2	0.380	48.38
γ=2	6	11979	28.0	3.4	0.800	87.12
	8	30375	20.5	3.5	0.339	85.24
	10	61731	18.5	7.1	0.139	41.99
	12	109503	18.0	11.0	0.044	27.31
	14	177147	18.0	16.4	0.046	18.31
γ=3	6	11979	20.0	7.3	0.080	41.15
	8	30375	18.0	6.8	0.085	44.09
	10	61731	19.5	15.1	0.116	19.83
	12	109503	20.5	23.8	0.141	12.59
	14	177147	25.0	35.1	0.150	8.53
Neighborhood distance $r_d = 1.1\Delta r_g$ γ=1	6	11979	24.0	11.8	1.926	25.49
	8	30375	19.5	6.2	0.647	48.15
	10	61731	18.5	5.4	0.519	55.96
	12	109503	18.0	5.7	0.390	52.42
	14	177147	18.0	7.2	0.308	41.37
γ=2	6	11979	20.5	12.8	0.628	23.50
	8	30375	18.0	8.0	0.270	37.51
	10	61731	17.5	9.7	0.133	30.92
	12	109503	17.0	12.5	0.059	23.98
	14	177147	17.0	17.3	0.030	17.35
γ=3	6	11979	17.5	21.1	0.122	14.19
	8	30375	17.0	11.5	0.022	25.97
	10	61731	16.0	17.4	0.018	17.25
	12	109503	16.0	26.5	0.015	11.31
	14	177147	15.0	36.4	0.009	8.23
Neighborhood distance $r_d = 1.5\Delta r_g$ γ=1	6	11979	19.5	29.4	1.177	10.21
	8	30375	20.5	14.9	0.467	20.14
	10	61731	18.5	9.8	0.372	30.44
	12	109503	17.5	8.5	0.296	35.40
	14	177147	17.5	9.0	0.247	33.33
γ=2	6	11979	20.0	29.7	0.289	10.09
	8	30375	17.5	16.0	0.089	18.68
	10	61731	16.0	14.3	0.085	20.90
	12	109503	16.0	15.3	0.055	19.58
	14	177147	17.0	19.2	0.033	15.60
γ=3	6	11979	17.5	31.5	0.155	9.52
	8	30375	16.0	20.1	0.018	14.94
	10	61731	16.0	21.9	0.016	13.68
	12	109503	15.0	28.1	0.009	10.65
	14	177147	16.0	38.6	0.007	7.76

TABLE III

COMPUTATION TIMES AND RELATIVE SPEEDUP FOR THE SMCG METHOD COMPARED TO THE FULL METHOD. FOR ALL CASES N_{cube}=15000

Memory requirements can be estimated by the number of expansion matrices $\overline{\overline{G}}_{\gamma_x\gamma_y\gamma_z}$ stored (times 2 including $\overline{x}$) multiplied by the length of each of those matrices given by Eq. (43). The memory required for the SMCG method is thus seen to be $\mathcal{O}(N)$ as compared to $\mathcal{O}(N^2)$ for the full method. As a final note, this SMCG algorithm is easily adapted to other types of particles such as spheres, crystals, dust grains, etc., for which the basis functions are known. This method may be used in a way which imitates the Discrete Dipole Approximation (DDA) [24,26,27], and the authors have used this method to find the effective permittivity of collections of randomly distributed spheroids [9].

V. CONCLUSIONS

The sparse matrix canonical grid (SMCG) method has been extended to 3-D and illustrated by finding the scattering from random media filled with dielectric spheroids at random positions and orientations. The 3-D SMCG method achieves $\mathcal{O}(N \log N)$ complexity instead of $\mathcal{O}(N^2)$ for the matrix-vector multiply when using an iterative solver by decomposing the interaction matrix $\overline{\overline{Z}}$, generated by an MoM solution to the many-body volume integral equation, into strong and weak interaction matrices $\overline{\overline{Z}}^{\mathrm{s}}$ and $\overline{\overline{Z}}^{\mathrm{w}}$, respectively. The matrix $\overline{\overline{Z}}^{\mathrm{s}}$ contains only those interactions which are between particles closer than the neighborhood distance r_d. Therefore, $\overline{\overline{Z}}^{\mathrm{s}}$ is very sparse and the matrix-vector multiply $\overline{\overline{Z}}^{\mathrm{s}} \cdot \overline{x}$ is accomplished in $\mathcal{O}(N)$ complexity. The matrix $\overline{\overline{Z}}^{\mathrm{w}}$ is formed by expanding the dyadic Green's function between each pair of particles whose associated gridpoints are located further apart than r_d in a γ^{th} order multivariate Taylor series expansion around a canonical grid superimposed onto the test volume. The prolate spheroidal particles considered in this paper were electrically small so that their response to electromagnetic excitation could be adequately approximated with a point response. Therefore, the Green's function interaction expansion matrices $\overline{\overline{G}}_{\gamma_x\gamma_y\gamma_z}$ exhibit a multilevel block Toeplitz (MBT) structure. MBT matrices can be multiplied with an arbitrary vector using the only one forward and one inverse FFT. Thus $\overline{\overline{Z}}^{\mathrm{w}} \cdot \overline{x}$ can be accomplished in $\mathcal{O}(N_T N \log N)$ complexity where N_T is the number of FFTs and depends on the expansion order γ. The 3-D SMCG method was demonstrated to indeed realize the predicted reduction in complexity and memory requirements through large-scale examples including up to 15000 discrete scatterers.

REFERENCES

[1] L. Tsang and J. A. Kong, "Multiple scattering of electromagnetic waves by random distributions of discrtet scatterers with coherent potential and quantum mechanical formulation," *Journal of Applied Physics*, vol. 51, no. 7, pp. 3465–3485, July 1980.

[2] L. Tsang and J. A. Kong, "Effective propagation constants for coherent electromagnetic wave propagation in media embedded with dielectric scatterers," *Journal of Applied Physics*, vol. 53, no. 11, pp. 7162–7173, November 1982.

[3] L. Tsang, J. A. Kong, K. H. Ding, and C. O. Ao, *Scatter-*

ing of Electromagnetic Waves: Numerical Simulations, Wiley-Interscience, 2000.

[4] A. Ishimaru, *Wave Propagation and Scattering in Random Media*, vol. 1 and 2, Academic, New York, 1978.

[5] R. F. Harrington, *Field Computation by Moment Methods*, Macmillan, New York, 1968.

[6] K. S. Yee, "Numerical solution of initial boundary value problems involving Maxwell's equations in isotropic media," *IEEE Transactions on Antennas and Propagation*, vol. 14, no. 3, pp. 302–307, Mar. 1966.

[7] A. Taflove, *Computational Electrodynamics: The Finite-Difference Time-Domain Method*, Artech House, Boston, 1995.

[8] L. Tsang, K. H. Ding, S. E. Shih, and J. A. Kong, "Scattering of electromagnetic waves from dense distributions of spheroidal particles based on Monte Carlo simulations," *Journal of the Optical Society of America A*, vol. 15, no. 10, pp. 2660–2669, October 1998.

[9] B. E. Barrowes, C. O. Ao, F. L. Teixeira, J. A. Kong, and L. Tsang, "Monte Carlo simulation of electromagnetic wave propagation in dense random media with dielectric spheroids," *IEICE Trans. on Electronics*, vol. E83-C, no. 12, pp. 1797–1802, December 2000.

[10] C. H. Chan, L. Li, and L. Tsang, "A banded matrix iterative approach to Monte Carlo simulations of large-scale random rough surface scattering: penetrable case," *9th Annual Review of Progress in Applied Computational Electromagnetics. Conference Proceedings. Appl. Comput. Electromagnetics Soc*, pp. 391–397, March 1993, Monterey, CA.

[11] V. Jandhyala, E. Michielssen, S. Balasubramaniam, and W. C. Chew, "A combined steepest descent-fast multipole algorithm for the fast analysis of three-dimensional scattering by rough surfaces," *IEEE Transactions on Geoscience and Remote Sensing*, vol. 36, no. 3, pp. 728–748, May 1998.

[12] L. Tsang, C. H. Chan, K. Pak, and H. Sangani, "A BMIA/FFT algorithm for the Monte Carlo simulations of large scale random rough surface scattering: application to grazing incidence," *IEEE Antennas and Propagation Society International Symposium 1994*, vol. 3, pp. 2028–2031, June 1994.

[13] L. Li, C. H. Chan, and L. Tsang, "Monte Carlo simulations of wave scattering from lossy dielectric random rough surfaces using the physics-based two-grid method and the canonical-grid method," *IEEE Transactions on Antennas and Propagation*, vol. 47, no. 4, pp. 752–763, April 1999.

[14] K. Pak, L. Tsang, and J. Johnson, "Numerical simulations and backscattering enhancement of electromagnetic waves from two-dimensional dielectric random rough surfaces with the sparse-matrix canonical grid method," *Journal of the Optical Society of America A*, vol. 14, no. 7, pp. 1515–1529, July 1997.

[15] S. Koc and W. C. Chew, "Multilevel FMA for the discrete dipole approximation," *IEEE Antennas and Propagation Society International Symposium*, vol. 1, pp. 640–643, 1999.

[16] W. C. Chew, J. M. Jin, C. C. Lu, E. Michielssen, and J. M. Song, "Fast solution methods in electromagnetics," *IEEE Transactions on Antennas and Propagation*, vol. 45, no. 3, pp. 533–543, March 1997.

[17] C. H. Chan and L. Tsang, "A sparse-matrix canonical-grid method for scattering by many scatterers," *Microwave and Optical Technology Letters*, vol. 8, no. 2, pp. 114–118, February 1995.

[18] J. T. Johnson, "On the canonical grid method for two-dimensional scattering problems," *IEEE Transactions on Antennas and Propagation*, vol. 46, no. 3, pp. 297–302, March 1998.

[19] S. Q. Li, Y. X. Yu, K. F. Chan, C. H. Chan, and L. Tsang, "A sparse-matrix/canonical grid method for analyzing densely packed interconnects," *IEEE Antennas and Propagation Society International Symposium*, vol. 1, pp. 128–131, 2000.

[20] S. Q. Li, C. H. Chan, M. Y. Xia, and L. Tsang, "Multilevel expansion of the sparse-matrix canonical grid method for two-dimensional random rough surfaces," *IEEE International Geoscience and Remote Sensing Symposium*, vol. 7, pp. 3111–3113, July 2000.

[21] L. Tsang, Jin A. Kong, and K. H. Ding, *Scattering of Electromagnetic Waves: Theories and Applications*, Wiley-Interscience, 2000.

[22] W. C. Chew, *Waves and Fields in Inhomogeneous Media*, Electromagnetic Waves. IEEE Press, 1995.

[23] J. van Bladel, "Some remarks on green's dyadic for infinite space," *IEEE Transactions on Antennas and Propagation*, vol. 9, pp. 563–566, 1961.

[24] B. E. Barrowes, F. L. Teixeira, and J. A. Kong, "Fast algorithm for matrix-vector multiply of asymmetric multilevel block-toeplitz matrices in 3-D scattering," *Microwave and Optical Technology Letters*, vol. 31, no. 1, pp. 28–32, Oct. 2001.

[25] T. M. Cover and J. M. Thomas, *Elements of Information Theory*, New York: Wiley, 1990.

[26] E. M. Purcell and C. R. Pennypacker, "Scattering and absorption of light by nonspherical dielectric grains," *Astrophysics Journal*, vol. 186, pp. 705–714, 1973.

[27] G. H. Goedecke and S. G. O'Brien, "Scattering by irregular inhomogeneous particles via the digitized Green's function algorithm," *Applied Optics*, vol. 27, no. 12, pp. 2431–2438, June 1988.

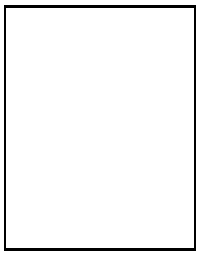

Benjamin E. BARROWES received his B.S. and M.S. degrees in Electrical Engineering from Brigham Young University both in 1999. He is currently pursuing the Ph.D. degree in Electrical Engineering from the Massachusetts Institute of Technology, Cambridge. His research interests include wind-wave interaction, electromagnetic wave scattering from the sea surface and from random media.

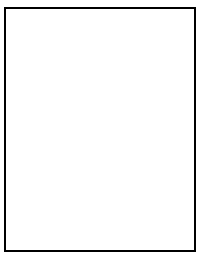

Chi O. AO received his A.B. degree in physics from the University of California at Berkeley in 1993 and his Ph.D. in physics from the Massachusetts Institute of Technology in 2001. He is currently a member of the Technical Staff at the Jet Propulsion Laboratory in Pasadena, California. He is co-author of the book *Scattering of Electromagnetic Waves: Numerical Simulations* (Wiley, 2001). His research interests include theoretical and numerical studies of wave scattering and propagation in geophysical media and their applications in remote sensing problems.

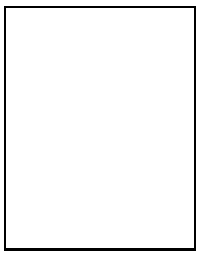

Fernando L. TEIXEIRA received the B.S. and M.S. degrees in electrical engineering from the Pontifical Catholic University of Rio de Janeiro (PUC-Rio), Brazil, in 1991 and 1995, respectively, and the Ph.D. degree in electrical engineering from the University of Illinois at Urbana-Champaign in 1999. From 1999 to 2000 he was a Postdoctoral Associate at the Research Laboratory of Electronics, Massachusetts Institute of Technology. Currently, he is an Assistant Professor at Department of Electrical Engineering, The Ohio State University, where he is also affiliated with the ElectroScience Laboratory. He is the editor of the book *Geometric Methods for Computational Electromagnetics* (EMW, Cambridge, 2001). His current research interests include analytical and numerical techniques for wave propagation and scattering in communication, sensing, and devices applications.

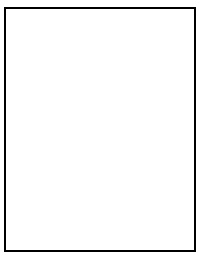

Jin A. KONG is a Professor of electrical engineering at the Massachusetts Institute of Technology (MIT), Cambridge. He has published eight books, including *Electromagnetic Wave Theory* (New York: Wiley, 1990), more than 400 refereed articles and book chapters, and super-vised more than 120 theses. He is Editor-in-Chief of the *Journal of Electromagnetic Waves and Applications*, Chief Editor of the book series *Progress in Electromagnetics Research*, and Editor of the *Wiley Series in Remote Sensing*. His research interests include electromagnetic wave theory and applications.